https://dx.doi.org/10.1016/j.engstruct.2019.02.022

Seismic fragility assessment of large-scale pile-supported wharf structures considering soil-pile interaction

Lei Su[1], Hua-Ping Wan[2*], You Dong[2], Dan M. Frangopol[3], Xian-Zhang Ling[1,4]

[1]School of Civil Engineering, Qingdao University of Technology, Qingdao, China

[2]Department of Civil and Environmental Engineering, The Hong Kong Polytechnic University, Kowloon, Hong Kong

[3]Department of Civil and Environmental Engineering, ATLSS Engineering Research Center, Lehigh University, Bethlehem, PA, USA

[4]School of Civil Engineering, Harbin Institute of Technology, Harbin, China

Abstract

Seismic fragility curves are recognized as a useful tool for seismic performance assessment of pile-supported wharf structure (PSWS) exposed to seismic hazards. These curves quantify the probability of structural vulnerability against given ground motion parameters. Soil-pile interaction (SPI) is found to have a significant impact on seismic performance of pile-supported structures. In this study, in order to better understand the SPI effect, the seismic fragility of a large-scale PSWS located at the Port of Los Angeles Berth 100, USA, is fully investigated with and without considering SPI. Herein, the pushover analysis scheme is used for inferring the bound limits of seismic demands of this large-scale PSWS. Specifically, the purpose of pushover analysis is twofold: to identify which pile of the PSWS most likely suffers from seismic failure; and to determine the bound limits of seismic demands for construction of seismic demand models using the identified pile. A collection of ground motions with low and high moment magnitudes as well as small and large epicentral

[*]Corresponding author.
E-mail address: sulei@qut.edu.cn (L. Su); huaping.wan@polyu.edu.hk (H.-P. Wan); you.dong@polyu.edu.hk (Y. Dong); dan.frangopol@lehigh.edu (D. M. Frangopol); lingxianzhang@qut.edu.cn (X.-Z. Ling).

distances are selected for nonlinear time history analysis. The fragility curves can be readily estimated from the data set of the intensity measure-seismic demand pairs by classical regression fitting. A comparison of fragility curves with and without SPI shows that SPI significantly influences the seismic fragility of the PSWS. For distinct damage states, the effect of SPI on the seismic fragilities of different piles can be totally different.

Keywords: Pile-supported wharf structure; Fragility; Soil-pile interaction; Pushover analysis; Nonlinear time history analysis

1 Introduction

Pile-supported wharf structures (PSWSs), which accommodate import and export activities, are essential components of a port transportation system to promote economic prosperity. Typically, a PSWS consists of one or more berths, and also include pile foundation, deck, and other necessary facilities for supporting the container. Many PSWSs are located in seismically active regions and are particularly vulnerable to damage and loss of function after a major earthquake. Damage to such structures has been frequently reported in many recent seismic events, such as the 1989 Loma Prieta [1], the 1995 Hyogoken-Nanbu earthquake [2], and the 2010 Haiti earthquake [3], among others. The resultant disruption in serviceability of PSWSs will have direct and detrimental impact on operation of the entire seaport leading to significant economic loss. To mitigate the potential seismic-induced damage to a PSWS, its seismic performance during earthquakes needs to be thoroughly assessed.

During the last two decades, a large volume of research work has been devoted to investigation of seismic performance of PSWSs using either model tests or numerical modeling. Model test schemes for characterizing the seismic response of PSWSs are mainly composed of centrifuge and full-scale field tests [4-9]. Boland et al. [4] performed a series of centrifuge model tests on PSWS to investigate the seismic response of wharf-ground system. Similarly, Takahashi and Takemura [5] explored the effect of liquefaction on the permanent displacement of wharf structure by centrifuge model test. Compared to the centrifuge model test, it is very hard that full-scale field test reproduced the global response of wharf structure. Roeder et al. [6] and Blandon et al. [7] conducted a large number of full-scale field test to investigate the seismic performance of pile-wharf connections. Chang et al. [8] carried out the in situ large-scale physical modeling on two-pile-supported wharf structure to study the dynamic soil-structure interactions using surface wave generator as an excitation. Boroschek et al. [9] performed a collection of ambient and forced vibration tests to characterize the damping properties of the PSWS. On the other hand, numerical modeling has also captured increasing attention of engineers to explore the seismic behavior of PSWS owing to its low cost and modeling generality. Compared to model tests, more work has been reported on using finite element (FE) analysis for seismic performance assessment of PSWSs [10-17]. Chiaramonte et al. [10] evaluated the full seismic performance of marginal wharves with both conventional and damage-resisting connections through a series of FE models. Shafieezadeh et al. [11] established two-dimensional nonlinear plane-strain model to investigate the model properties and vulnerability of PSWS and found that the failure of PSWS mainly contributed to lateral permanent deformation of deck, damage of pile-deck connection, and tensile axial force of batter piles. Shafieezadeh et al. [12] and Su et al. [13] fully explored the seismic performance of PSWSs by building a three-dimensional (3D) nonlinear FE model considering complex interaction between the surrounding soil, pile foundation, and wharf structure. Doran et al. [14] evaluated the seismic performance of two existing PSWSs through nonlinear static pushover analysis according to the Turkish Code for Shore Structures. Erdogan et al. [15] assessed the seismic performance of aging PSWS with two retrofitting schemes of arranging the additional piles. Donahue et al. [16] studied the seismic performance of a PSWS by numerical model validated using the recorded strong motion data. Su et al. [17] investigated the influence of model parameter uncertainty on seismic responses of the PSWS through the computationally efficiently surrogate modeling technique. In spite of substantial investigations on assessment of PSWSs using either model tests or numerical simulations, very limited studies have been reported regarding seismic fragility evaluation of PSWSs. The seismic fragility function, which is defined as the relationship between the conditional probability of exceeding a specified structural damage state and the ground motion intensity measure, has been widely recognized as a practical and effective tool for evaluating the seismic vulnerability of infrastructure systems, such as bridges [18-25] and buildings [26-30]. The few relevant studies on seismic fragility assessment of wharf structure are mentioned in sequence. For example, Calabrese and Lai [31] carried out seismic fragility assessment of the blockwork wharf structure based on the artificial neural networks and found that the liquefaction and the base width-height ratio would increase the failure probabilities. Alielahi and Rabeti Moghadam [32] evaluated the seismic fragility of the broken-back block quay walls using numerical models validated against the shaking table test results. It was found that the quay wall with larger hunch has the better seismic performance. Yang et al. [33] studied seismic fragility curves for PSWSs with vertical piles by performing nonlinear time history analysis conducted with the OpenSees FE platform. Chiou et al. [34] proposed a procedure of developing fragility curves for a typical PSWS in Taiwan through pushover analysis. Heidary-Torkaman et al. [35, 36] assessed fragility of a PSWS with batter piles through a practical framework, and they also carried out sensitivity analysis to measure the effects of structural properties on seismic performance. Balomenos and Padgett [37] conducted fragility analysis of PSWS with four alternative pile-deck connections subjected to hurricane-induced storm surge and wave loading. The results revealed that the uplift was the dominant structural failure mode of PSWS under the extreme hazard conditions.

PSWS is a typical pile-supported structure system, so the soil-pile interaction (SPI) is involved and will affect the seismic performance. Traditionally, SPI has been considered to be beneficial for seismic design since it elongates the period of the structure and increases the damping of the structural system [38, 39]. However, the perceived beneficial role of SPI has been challenged because it is drawn from oversimplification of the reality and indeed is incorrect for certain structure systems and earthquake motions [40, 41]. Zhang and Tang [42] maintained that the beneficial or detrimental role of SPI in seismic response strongly depends on structure-to-earthquake frequency ratio, foundation-to-structure stiffness ratio, damping coefficient of foundation impedance, foundation rocking, and the development of nonlinearity in structures. SPI is an important issue, especially for stiff and large pile-supported structures located in soft clay or liquefiable soil [43-45]. These research findings highlight the significance of incorporation of SPI in seismic performance assessment of pile-supported structures. Therefore, seismic fragility evaluation of the PSWS is implemented with consideration of the SPI effect.

In this study, the seismic fragility of a large-scale PSWS located at the Port of Los Angeles Berth 100 is studied. The FE model of this PSWS is established using the OpenSees computer program. The modeling of soil-pile interface is detailed on how to account for SPI in FE model. A pushover analysis is used to determine the bound limits of demand parameters of the wharf structure. Pushover analysis provides an effective means to calculate the quantitative seismic demands. A suite of ground motion records are adopted to evaluate the seismic performance of the PSWS by performing the nonlinear time history analysis. The seismic demand models of the PSWS with and without SPI are constructed from the obtained data set of the intensity measure-seismic demand pairs. Using the seismic demand models and appropriate bound limits of damage states, seismic fragility curves with and without SPI are evaluated. The influence of the SPI on the seismic fragility curves of this large-scale PSWS is thoroughly investigated. In summary, the contribution of this work is twofold: (1) the powerful pushover analysis procedure is utilized to precisely determine the bound limits of demand parameters associated with various damage states; and (2) the seismic fragility of the large-scale PSWS with and without considering the SPI effect is systematically investigated.

2 Wharf Structure and Finite Element Modeling

2.1 Description of wharf structure

A large-scale PSWS located at port of Los Angeles Berth 100 is under investigation. Fig. 1 shows the 3D profile of such container wharf and pile modeling. Additional details can be found in the references [13, 46]. This target wharf structure is 317 m long and 30.5 m wide. Along the longitudinal direction, there are a total of 52 bays with an identical distance of 6.1

m in between (Fig. 1a), and along the transverse direction, there exist six rows of prestressed reinforced concrete piles. To be more specific, each pile is 42 m long, and the distance between the pile rows F and E is 3.7m (Fig. 2a), while the distance between the remaining pile rows is 6.7 m. The pile rows F and E have an identical depth in the ground whereas the rest have various underground depths. The concrete deck supported on these piles is at least 0.4 m thick. The dike, aiming at improving the stability of this large-scale PSWS, has an inclination of 31 degree. According to configuration of the wharf structure, a representative slice with unit width selected for simulation is shown in Fig. 1(a).

2.2 Piles modeling

The pile section has an octagonal shape whose sides are around 0.253 m long and its fiber discretization is shown in Fig. 1(b) and (c). The fiber section of the pile consists of the core and cover concretes, and steel reinforcement bars. The uniaxial Kent-Scott-Park concrete model with degraded linear unloading/reloading stiffness (i.e., *Concrete01* material in OpenSees) is used to model the core and cover concretes, and the uniaxial Giuffre-Menegotto-Pinto model with isotropic strain hardening (i.e., *Steel02* material in OpenSees) is utilized to simulate the steel reinforcement bars. Note that an initial strain is applied to consider the prestressing effect of steel reinforcement bars. The properties of concrete and steel in fiber section are listed in Table 2 and their strain-stress responses are shown in Fig. 1(d), (e) and (f). The behavior of moment-curvature of the prestressed reinforced concrete pile cross section is shown in Fig. 1(g), which demonstrates that the nonlinear behavior of pile cross section is obvious, and the initial stiffness is very large because of prestressing. The bending moment starts to decline after reaching the peak, and then it has a slight increment. In this regard, the prestressed RC piles are modeled using nonlinear force-based beam-column elements with fiber section. The wharf deck is modeled using linear elastic beam elements.

3.3 Soil domain modeling

Since the lateral boundary is far from the PSWS and a wide range of FE types are used to model this pile-supported wharf-ground system, the target FE simulation domain is selected as shown in Fig. 2(a). The configuration details of the wharf structure are provided in Fig. 2(a). Specifically, the length of FE model is 230 m, its height is 53.8 m at the landside, and 33.5 m at the waterside for soil profile (Fig. 2a). The resulting FE model of the wharf structure is shown in Fig. 2(b). The completed FE model has a total of 1393 nodes and 1305 elements, including 1186 soil elements and 119 nonlinear beam-column elements.

The whole soil domain is idealized into four units including 9 sub-layers as well as the dike structure shown in Fig. 2(a), in which distinct colors stand for different soil layers. The properties of soil stratum are tabulated in Table 1. The saturated soil is modeled using four-node plane-strain bilinear isoparametric elements which allow for characterization of the dynamic behavior of two-phase solid-fluid fully coupled material [47]. Each node of this element has three degree-of-freedom (DOF), two of which represent the solid displacement and one represents the fluid pressure. Note that in the FE modeling, a high permeability (i.e., 1 m/s) is adopted to prevent the liquefaction since with the relatively high friction angle for sand stratum (Table 1), the liquefaction is not a main problem. The water level is located on the top of loose marine sand (IIA, shown in Fig. 2a). The water body is simulated through applying the hydrostatic pressure on the ground surface at the waterside. The average nodal loads resulting from the water weight above the soil surface is taken into account to precisely determine the effective stresses on the soil layer [48]. Actually, the soil stratum has the stress and pore pressure fields but with zero displacement field under the soil gravity. Fortunately, the OpenSees computer program is able to ensure the zero displacement of FE model in the gravity phase [49]. In this regard, two gravity runs are performed to achieve this purpose: (1) the 1st gravity run is conducted to obtain non-zero stress, pore pressure, and displacement fields by activating the initial state analysis feature; and (2) the 2nd gravity run is carried out to achieve the zero-displacement field while maintaining stress and pore pressure field with the initial state analysis feature off.

3.4 Soil-pile interaction modeling

For this PSWS, the involved SPI effect should be taken into account in the numerical modeling. The SPI is generally a very critical and complex dynamic interaction, especially for the large-scale pile-supported structures. Desai and Nagaraj [50] investigated the four types of possible deformation mechanism on soil-pile interface. Based on these mechanisms, the interface element was developed to simulate the SPI by researchers. For example, Elgamal et al. [51] employed the rigid link element perpendicular to pile axis with equalDOF constraints (i.e., *equalDOF* in OpenSees), which directly connect the soil node and the end node of rigid link element (Fig. 3). To be specific, the node A(B) directly connects to the corresponding node A'(B') by equalDOF. Such interface modeling can incorporate the effect of pile geometry but fails to characterize the friction and slip mechanism of soil-pile interface during dynamic excitation [51]. Therefore, such modeling scheme is still considered as numerical modeling without SPI since it fails to properly account for the SPI effect. Its modeling capability can be improved to simulate the friction and slip effect of SPI. Specifically, the zero-length element are added to links A(B) and A'(B'). This connection is created by the equal DOF constraint, zero-length element, and elastic beam. In this regard, the zero-length element provides the yield shear force, perpendicular to the axial force to simulate the slip at the soil-pile interface. The schematic soil-pile interface connection is shown in Fig. 3. More details regarding modeling soil-pile interface with SPI are provided in Su et al. [13].

3.5 Boundary and loading conditions

The boundary conditions of the FE model are: (1) lateral boundary is applied by employing the larger soil column to ensure that free-field conditions; (2) before shaking, the nodes at the bottom of the model are fixed in all directions during shaking, the lateral displacement DOF constraint in the shaking direction is released; and (3) the nodal pore pressure is specified on the ground surface at the waterside in line with the water height so that the ground surface boundaries at the waterside and landside are pervious.

Both linear and nonlinear analyses are involved for the FE modeling of this wharf-ground system. In a linear analysis, a gravity application analysis (self-weight modeling) is performed before seismic excitation. Subsequently, the initial state analysis is conducted to maintain the soil stress states and make the soil displacement zero through the OpenSees *InitialStateAnalysisWrapper* [49]. The obtained soil stress states are used as the initial conditions for the subsequent dynamic analysis. Following the procedures described by Chiaramonte [52], the following staged analysis runs are employed to achieve the convergence and model the actual loading conditions:

(1) The self-gravity of model is performed to obtain the initial stress state (i.e., zero displacement and non-zero stress and pore pressure) for the subsequent analysis shown in Fig. 4(a).

(2) The static analysis of pile foundations simulated by nonlinear beam-column element based on fiber section is conducted. At this run, the pile bottom is fixed and the prestressing force is applied to make pile foundations deform freely as shown in Fig. 4(b).

(3) The linear elastic beam elements and interface element (i.e., *zeroLength* and *zeroLengthSection* elements in OpenSees) are added to simulate the deck and soil-pile interaction, respectively. The constraints applied to pile bottom are removed while the constraints on other end of zero-length elements are added (Fig. 4c). Then the static analysis is conducted. It should be noted that the soil and pile meshes are independent of each other in this phase.

(4) The constraints on the zero-length elements are removed and the free nodes of zero-length elements are connected to the corresponding soil nodes through the equalDOF (Fig. 4d). The self-gravity of deck and pile are applied, followed by static analysis.

(5) The properties of soil layers switch from elastic to plastic, and then the plastic analysis is performed, shown in Fig. 4(e).

(6) The soil column with heavy mass are connected with both sides of model through the equalDOF to simulate the free field boundary. Finally, after applying the base motion, the nonlinear time history analysis is conducted to calculate the seismic response (Fig. 4f).

3 Seismic Demand Models

As recommended by Ramanathan et al. [53] and Zhong et al. [21], a suite of 80 ground motions are selected for seismic time history analysis. These ground motions are extracted from the Pacific Earthquake Engineering Research Center Strong Motion Database [54]. The ground motion selection criteria are: (1) the California ground motions recorded on site class D are under consideration since the wharf is located in California and its site type belongs to class D; and (2) the chosen ground motions should have various moment magnitudes as well as fault distances to be more representative. Specifically, the selected 80 ground motions are from California earthquakes recorded on site class D with moment magnitude between 5.8 and 6.9 and fault distance from 13 to 60 km. For more details on characteristics of ground motions, interested readers are referred to [54]. For this wharf structure, the seismic demands (responses) of interest consist of deck displacement, bending moment and curvature on pile top. Seismic demand model is to map the relationship between intensity measure (*IM*) and seismic demand (*D*). In general, the seismic demand model is derived by regression fitting in a logarithmic space, that is, determination of the ln(*IM*)-ln(*D*) relationship [55]. In the numerical modeling of this wharf structure, the velocity time histories along with dashpot are imparted as the base motion. In addition, the peak ground velocity (PGV) is one of most widely used *IM*s for seismic performance assessment of geotechnical engineering structures [56, 57]. Thus, PGV is chosen as *IM* for construction of seismic demand models of this wharf structure. Following the above-mentioned FE modeling procedures, nonlinear time history analysis is conducted for each of the selected 80 ground motions to obtain interested seismic responses. Note that nonlinear time history analysis is performed on the FE model with and without SPI. Eventually, a data set is collected with 80 input-output pair for both cases with and without SPI. The seismic demand models of the wharf structure can be readily derived by regression method using the obtained data set. The results are showed in Figs. 5-7.

Fig. 5 demonstrates the seismic demand model of deck displacement w.r.t. *IM* of PGV with and without SPI in the logarithm scale. Noted that the deck displacement is recorded at the leftmost end of deck (i.e., the top of Pile F). Apparently, the log-linear model fit the samples well, indicating the effectiveness of the adopted linear model in determination of seismic demand models. It can also be seen that for the deck displacement, seismic demand model with SPI is very similar to the one without SPI, which indicates that the SPI has little effect on the deck displacement. Fig. 6 depicts the seismic demand models associated with bending moment on the top of different piles with and without SPI. Unlike the deck displacement, the SPI obviously influences the bending moment on pile top. Actually, the difference between seismic demand models with and without SPI are more pronounced when the fit models are plotted in normal scale instead of in logarithmic scale. As seen from Fig. 6, the slope of the log-linear seismic demand model decreases from Piles A to F, which reveals the decreasing sensitivity of bending moment on pile top to PGV. Fig. 7 illustrates the seismic demand models associated with the curvature on the top of different piles with and without SPI. Similarly, the SPI has significant impact on the curvature on pile top.

4 Seismic Fragility Evaluation

4.1 Damage state classification by pushover analysis

Determination of proper quantitative damage demands is essential for seismic fragility evaluation. The International Navigation Association presents the qualitative demands to classify the damage states of PSWS [58], but the quantitative demands are not available. As stated by Chiou et al. [34], pushover analysis is a powerful tool to determine the qualitative demands associated with different damage states of PSWS. Therefore, a nonlinear static pushover analysis is conducted primarily for fragility evaluation. Such analysis procedure is employed to determine bound limits of seismic demands for the slight, moderate, and extensive damage states. This analysis is performed through gradually increasing the lateral displacement of wharf deck. The increased lateral displacement can induce the increase of concrete strain sequentially as well as the transition from slight damage state to extensive one. The bound limits of demand parameters are identified by the relationships between concrete strain and demand parameters established by the pushover analysis. The pushover procedure for determining the bound limits of seismic demands of different damage states consists of two steps. The first step is to identify which structural component (i.e., pile here for the PSWS) is most likely to be damaged, and the second step is to determine the bound limits based the relationship between the concrete strain and seismic demands of the identified pile. A general flowchart for the bound limit determination of seismic demands based on pushover analysis is shown in Fig. 8.

The pushover results are shown in Figs. 9 and 10. Fig. 9 shows the pushover bending moment-curvature responses on the pile top with and without SPI. It is shown that the bending moment-curvature responses on pile top with and without SPI are very similar to that of fiber section (Fig. 1g), which confirms the reliability of the established numerical model. Additionally, the pile top section presents an obvious nonlinear characteristic, and the nonlinear behavior is more pronounced for the piles with shorter free length because of larger lateral force and curvature on the pile. The bending moment-curvature response without SPI is larger than that with SPI, especially for the Piles E and F. Fig. 10 depicts the pushover force-displacement responses on pile top with and without SPI. Similarly, for the lateral force-displacement of isolated pile (Fig. 10a), the lateral force without SPI is greater than that with SPI, especially for Piles E and F. Since the free lengths of the piles decrease from the Piles A to F, their lateral forces decrease. To further explore the effect of SPI, the total lateral force-displacement is also calculated, as shown in Fig. 10(b). Once again, the total lateral force without SPI is significantly larger than that with SPI for the same deck displacement. It can be concluded from Figs. 9 and 10 that the SPI has substantial influence on the moment-curvature response and force-displacement response. Given the fact that the pushover responses of the Pile F are largest among all piles with and without SPI, the seismic responses of the Pile F will be used to determine the bound limits of seismic demands.

Likewise, the pushover analysis is conducted again only for the target Pile F. The results are shown in Fig. 11, which depicts the relationship between the demand parameters and the concrete strain. Given the concrete strain at different damage states, the strain-seismic demand relationship can be utilized to infer the corresponding bound limits of the demand parameters. Three damage states including slight, moderate, and extensive levels are considered for seismic fragility evaluation. In particular, the slight damage state corresponds to the core concrete strain at compressive strength (i.e., 0.005 in Table 2); the extensive damage state corresponds to the core concrete strain at crushing strength (i.e., 0.018 in Table 2); and the moderate damage state is assumed to be the core concrete strain of 0.01, which is close to the average of the slight and extensive damage levels. These concrete strains associated with three damage states are entered into the strain-seismic demand relationship function to calculate the bound limits of the seismic demand parameters. Table 3 summaries the bound limits of the seismic demand parameters of the PSWS under different damage states.

4.2 Determination of seismic fragility curve

The fragility curve is defined as the conditional probability that the seismic demand (D) exceeds its bound limit of demand parameters (L) for a given IM as

$$P\left(D \geq L \middle| IM\right) = \Phi\left[\frac{\ln\left(S_D\right) - \ln\left(S_L\right)}{\sqrt{\beta_{D|IM}^2 + \beta_L^2}}\right] \tag{1}$$

where S_D is the median estimate of the demand as a function of IM; S_L is the median estimate of the bound limit of seismic demand; $\beta_{D|IM}$ is the dispersion or logarithmic standard deviation of the demand conditioned on IM; β_L is the dispersion of the bound limit of seismic demand; and $\Phi(\bullet)$ denotes the cumulative standard normal distribution function.

Thus, the fragility for any structural component of the wharf structure can be estimated if the governing parameters S_D, S_L, $\beta_{D|IM}$, and β_L are first determined. Specifically, S_D is determined based on the seismic demand models shown in Figs. 5-7; S_L is determined based on pushover analysis results listed in Table 3; β_L is assumed to be 15%; and the last quantity $\beta_{D|IM}$ is computed through the following expression

$$\beta_{D|IM} = \sqrt{\frac{\sum_{i=1}^{N}\left[\ln\left(d_i\right) - \ln\left(S_D\right)\right]^2}{\left(N-2\right)}} \tag{2}$$

where d_i is the ith demand for the ith ground motion; and N is the number of the selected ground motions.

4.3 Results of seismic fragility analysis

Base on the fragility analysis, fragility curves of the wharf structure are obtained as shown in Figs. 12-14. The fragility curves associated with the deck displacement-specific seismic demand are compared in Fig. 12, which provides a clear picture of how damage exceedance probability (fragility) for each damage responses to the different PGV levels with and without SPI. For example, with consideration of SPI, the fragilities of the wharf deck are 98.6%, 61.1%, and 12.0% for the slight, moderate, and extensive damage states, respectively, when the PGV is specified as 0.5 m/s. As shown in Fig. 12, the wharf deck has less seismic vulnerability when considering SPI, especially for extensive damage state. For strong intensity of the ground motions, such as PGV of 0.8 m/s, the probability of the extensive damage state without SPI is 92.5% while the damage probability with SPI is only 62.7%. It can also be found that the difference between the fragility curves with and without SPI becomes more significant from small to large damage states. These observations indicate that SPI has critical effect on fragility of the wharf deck, and the design of PSWS will be conservative if the SPI effect is neglected.

Fig. 13 presents the fragility curves of bending moments on the top of different piles. Unlike the deck displacement, the fragility curves of bending moments with SPI are not always over or below those without SPI. For the Piles A, E, and F, the fragilities with and without SPI have the same feature for each damage state, so do the remaining piles. Overall, the fragilities with SPI are larger than those without SPI under the moderate and extensive damage states and their difference becomes more obvious from the moderate to extensive damage states. However, under the slight damage state, fragilities with SPI are either larger or smaller than those without SPI for different piles.

Fig. 14 shows the fragility curves of curvatures on the top of different piles. It is clear that for all three damage states of Piles A-D, fragilities with SPI are greater than those without SPI. This indicates that when the SPI effect is not taken into account, the damage probability will be underestimated. The fragility increases from Piles A to F is inversely proportional to the free length of piles. This observation may indicate that the fragilities of bending moments increase with the decrease of the free length of piles. Under the slight damage state, the difference between fragilities with and without SPI is relatively small, especially for the Piles D-F. On the other hand, the difference between fragilities with and without SPI becomes more significant from the moderate to extensive damage states. Overall, the damage probability for the Piles E and F is larger than that for the Piles A-D, which infers that the piles with shorter free length are more vulnerable to damage during earthquake. Like the bending moments, the SPI can have either negative or positive impact on the fragilities of curvatures associated with different damage states for different piles.

In summary, the SPI significantly influences the fragilities of the wharf structure. The SPI effect on the fragilities associated with different seismic demands (e.g., deck displacement and bending moment) can be totally distinctive. The SPI can have either negative or positive impact on the fragilities for different structural components and different damage states. For this reason, a reliable estimate of the fragilities of the wharf structures is necessary.

4.4 Discussion

The above results of seismic fragility analysis illustrate the damage exceedance probability of PSWS for various damage states with and without SPI. For deck displacement, the seismic fragility without SPI is obviously larger than that with SPI (Fig. 12). Overall, the seismic fragility without SPI is smaller for bending moment and curvature of the pile, compared to the case with SPI (Figs. 13-14). In other words, the effect of SPI decreases the deck displacement-specific seismic fragility but the bending moment and curvature-specific ones. Such phenomenon may be explained by the fact that the wharf system without SPI is more rigid, which leads to the small deck displacement and the large bending moment and curvature. In contrast, the wharf system with SPI is more flexible, and thus, it has a relative great deck displacement and small bending moment and curvature. The characteristics of the wharf system with and without SPI can be confirmed by the pushover analysis results (Fig. 11). Fig. 11 indicates that under the same concrete strain, the wharf system without SPI produces the smaller deck displacement and larger bending moment and curvature than the wharf system with SPI. As a result, the discrepancy in the effect of SPI on the displacement-specific seismic fragility versus the bending moment- and curvature-specific seismic fragility is obtained.

5 Conclusionsq

Seismic fragility curves, which defines the probability of reaching or exceeding a specified damage state given different ground motion intensity measures, are very powerful tools for seismic vulnerability assessment. Soil-pile interaction (SPI) has been found to have a significant impact on seismic performance of pile-supported wharf structures (PSWSs). SPI is a complex process involving inertial and kinematic interaction between piles and soil, time-varying pore-water pressure, and soil nonlinearity. In this study, the focus is placed on seismic fragility evaluation of the PSWS as well as on the SPI effect. Specifically, the seismic fragility of a large-scale PSWS located at the Port of Los Angeles Berth 100 is fully investigated with and without considering SPI. In addition, to accurately classify the different damage states for fragility assessment, the pushover analysis strategy is utilized to determine the bound limits of seismic demands of this large-scale PSWS.

The key findings are as follows:

- Pushover analysis provides a reliable tool for damage state classification. It is not only able to detect which pile of the PSWS is most likely to fail under seismic actions, but also effective for inferring the bound limits of seismic demands.
- SPI has a significant effect on the pushover responses of the piles of the PSWS. It is found that the difference between the pile pushover responses with and without SPI is particularly substantial for the most likely damaged Pile F.
- SPI significantly affects the seismic fragilities of the PSWS. The discrepancy between the fragility curves with and without SPI becomes more noticeable from small to large damage states, which tell modelers that more close attention should be paid to the SPI effect when assessing seismic fragilities of the PSWS under extensive damage state.
- SPI can have either negative or positive impact on the seismic fragilities for different structural components and different damage states. Therefore, for different structural components and different damage states, seismic fragility with SPI can be either smaller or larger than the one without SPI. For this reason, a reliable estimate of the fragilities of the wharf structures is necessary.

Acknowledgements

This research was financially supported by the National Natural Science Foundation of China (51808307 and 51878235), the National Key Research and Development Program of China (2016YFE0205100), the Shandong Provincial Natural Science Foundation, China (ZR2017QEE007), and the Special Project Fund of Taishan Scholars of Shandong Province, China (2015-212).

References

[1] EQE. The October 17, 1989 Loma Prieta Earthquake. Prepared by EQE Engineering Inc. Report, October 1989.

[2] Chung RM. The January 17, 1995 Hyōgo-ken-Nanbu (Kobe) Earthquake: Performance of structures, lifelines, and fire protection systems. US Department of Commerce, Technology Administration, National Institute of Standards and Technology, 1996.

[3] Green RA, Olson SM, Cox BR, Rix GJ, Rathje E, Bachhuber J, French J, Lasley S, Martin N. Geotechnical aspects of failures at Port-au-Prince Seaport during the 12 January 2010 Haiti Earthquake. Earthquake Spectra 2011; 27(S1):43-65.

[4] Boland JC, Schlechter SM, McCullough NM, Dickenson SE, Kutter BL, Wilson DW. Data report: Pile-supported wharf centrifuge model (SMS02). Center for Geotechnical Modeling. University of California at Davis, 2001.

[5] Takahashi A, Takemura J. Liquefaction-induced large displacement of pile-supported wharf. Soil Dynamics and Earthquake Engineering 2005; 25(11):811-825.

[6] Roeder CW, Graff R, Soderstrom J, Yoo JH. Seismic performance of pile-wharf connections. Journal of Structural Engineering 2005; 131(3):428-437.

[7] Blandon CA, Bell JK, Restrepo JI, Weismair M, Jaradat O, Yin P. Assessment of seismic performance of two pile-deck wharf connections. Journal of Performance of Constructed Facilities 2010; 25(2):98-104.

[8] Chang WJ, Chen JF, Ho HC, Chiu YF. In situ dynamic model test for pile-supported wharf in liquefied sand. Geotechnical Testing Journal 2010; 33(3):212-224.

[9] Boroschek RL, Baesler H, Vega C. Experimental evaluation of the dynamic properties of

a wharf structure. Engineering Structures 2011; 33(2):344-356.

[10] Chiaramonte Maurizio M, Arduino P, Lehman Dawn E, Roeder Charles W. Seismic analyses of conventional and improved marginal wharves. Earthquake Engineering & Structural Dynamics 2013; 42(10):1435-1450.

[11] Shafieezadeh A, DesRoches R, Rix GJ, Werner SD. Seismic performance of pile-supported wharf structures considering soil-structure interaction in liquefied soil. Earthquake Spectra 2012; 28(2):729-757

[12] Shafieezadeh A, DesRoches R, Rix GJ, Werner SD. Three-dimensional wharf response to far-field and impulsive near-field ground motions in liquefiable soils. Journal of Structural Engineering 2012; 139(8):1395-1407.

[13] Su L, Lu J, Elgamal A, Arulmoli AK. Seismic performance of a pile-supported wharf: Three-dimensional finite element simulation. Soil Dynamics and Earthquake Engineering 2017; 95:167-179.

[14] Doran B, Shen J, Akbas B. Seismic evaluation of existing wharf structures subjected to earthquake excitation: Case study. Earthquake Spectra 2013; 31(2):1177-1194.

[15] Erdogan H, Doran B, Seckin A, Akbas B, Celikoglu Y, Bostan T. Seismic performance and retrofit evaluation of an existing pile-wharf structure. Journal of Performance of Constructed Facilities 2017; 31(6):04017110.

[16] Donahue MJ, Dickenson SE, Miller TH, Yim SC. Implications of the observed seismic performance of a pile-supported wharf for numerical modeling. Earthquake Spectra, 2005; 21(3):617-634.

[17] Su L, Wan HP, Dong Y, Frangopol DM, Ling XZ. Efficient uncertainty quantification of

wharf structures under seismic scenarios using Gaussian process surrogate model. Journal of Earthquake Engineering 2018; 1-22

[18] Li C, Li HN, Hao H, Bi K, Chen B. Seismic fragility analyses of sea-crossing cable-stayed bridges subjected to multi-support ground motions on offshore sites. Engineering Structures 2018; 165:441-456.

[19] Dong Y, Frangopol D M, Saydam D. Time-variant sustainability assessment of seismically vulnerable bridges subjected to multiple hazards. Earthquake Engineering & Structural Dynamics 2013; 42(10):1451-1467.

[20] Ramanathan K, Padgett JE, DesRoches R. Temporal evolution of seismic fragility curves for concrete box-girder bridges in California. Engineering Structures 2005; 97:29-46.

[21] Zhong J, Jeon JS, Yuan W, DesRoches R. Impact of spatial variability parameters on seismic fragilities of a cable-stayed bridge subjected to differential support motions. Journal of Bridge Engineering 2017; 22(6):04017013.

[22] Dong Y, Frangopol DM. Probabilistic assessment of an interdependent healthcare-bridge network system under seismic hazard. Structure and Infrastructure Engineering 2017; 13(1):160-170.

[23] Dong Y, Frangopol DM. Probabilistic time-dependent multihazard life-cycle assessment and resilience of bridges considering climate change. Journal of Performance of Constructed Facilities 2016; 30(5):04016034.

[24] Dong Y, Frangopol DM. Risk and resilience assessment of bridges under mainshock and aftershocks incorporating uncertainties. Engineering Structures 2015; 83:198-208.

[25] Zheng Y, Dong Y, Li Y. Resilience and life-cycle performance of smart bridges with

shape memory alloy (SMA)-cable-based bearings. Construction and Building Materials 2018; 158:389-400.

[26] Sasani M, Der Kiuregian A. Seismic fragility of RC structural walls: Displacement approach. Journal of Structural Engineering 2001; 127(2):219-228.

[27] Seyedi DM, Gehl P, Douglas J, Davenne L, Mezher N, Ghavamian S. Development of seismic fragility surfaces for reinforced concrete buildings by means of nonlinear time-history analysis. Earthquake Engineering & Structural Dynamics 2010; 39(1):91-108.

[28] Babič A, Dolšek M. Seismic fragility functions of industrial precast building classes. Engineering Structures 2016; 118:357-370.

[29] Ji J, Elnashai AS, Kuchma DA. An analytical framework for seismic fragility analysis of RC high-rise buildings. Engineering Structures 2007; 29(12):3197-3209.

[30] Dong Y, Frangopol DM. Performance-based seismic assessment of conventional and base-isolated steel buildings including environmental impact and resilience. Earthquake Engineering & Structural Dynamics 2016; 45(5):739-756.

[31] Calabrese A, Lai CG. Fragility functions of blockwork wharves using artificial neural networks. Soil Dynamics and Earthquake Engineering 2013; 52:88-102.

[32] Alielahi H, Rabeti Moghadam M. Fragility curves evaluation for broken-back block quay walls. Journal of Earthquake Engineering 2017; 21(1):1-22.

[33] Yang CSW, DesRoches R, Rix GJ. Numerical fragility analysis of vertical-pile-supported wharves in the western United States. Journal of Earthquake Engineering 2012; 16(4):579-594.

[34] Chiou JS, Chiang CH, Yang HH, Hsu SY. Developing fragility curves for a

pile-supported wharf. Soil Dynamics and Earthquake Engineering 2011; 31(5-6):830-840.

[35] Heidary-Torkamani H, Bargi K, Amirabadi R. Seismic vulnerability assessment of pile-supported wharves using fragility curves. Structure and Infrastructure Engineering 2014; 10(11):1417-1431.

[36] Heidary-Torkamani H, Bargi K, Amirabadi R, McCllough NJ. Fragility estimation and sensitivity analysis of an idealized pile-supported wharf with batter piles. Soil Dynamics and Earthquake Engineering 2014; 61-62:92-106.

[37] Balomenos GP, Padgett JE. Fragility analysis of pile-supported wharves and piers exposed to storm surge and waves. Journal of Waterway, Port, Coastal, and Ocean Engineering 2018; 144(2):04017046.

[38] Jennings PC, Bielak J. Dynamics of building-soil interaction. Bulletin of the Seismological Society of America 1973; 63(1):9-48.

[39] Veletsos AS, Meek JW. Dynamic behaviour of building-foundation systems. Earthquake Engineering & Structural Dynamics 1974; 3(2):121-138.

[40] Bielak J. Dynamic behaviour of structures with embedded foundations. Earthquake Engineering & Structural Dynamics 1974; 3(3):259-274.

[41] Mylonakis G, Gazetas G. Seismic soil-structure interaction: beneficial or detrimental?. Journal of Earthquake Engineering 2000; 4(03):277-301.

[42] Zhang J, Tang Y. Dimensional analysis of structures with translating and rocking foundations under near-fault ground motions. Soil Dynamics and Earthquake Engineering 2009; 29(10):1330-1346.

[43] Boulanger RW, Curras CJ, Kutter BL, Wilson DW, Abghari A. Seismic soil-pile-structure interaction experiments and analyses. Journal of Geotechnical and Geoenvironmental Engineering 1999; 125(9):750-759.

[44] Maheshwari BK, Truman KZ, El Naggar MH, Gould PL. Three-dimensional nonlinear analysis for seismic soil-pile-structure interaction. Soil Dynamics and Earthquake Engineering 2004; 24(4):343-356.

[45] Rodriguez ME, Montes R. Seismic response and damage analysis of buildings supported on flexible soils. Earthquake Engineering & Structural Dynamics 2000; 29(5):647-665.

[46] EMI. Final geotechnical and seismic analyses and design report berth 100 container wharf, west basin Port of Los Angeles, San Pedro, California. Prepared by Earth Mechanics, Inc. (EMI) submitted to Port of Los Angeles, California, 2001.

[47] Yang Z, Elgamal A. Influence of permeability on liquefaction-induced shear deformation. Journal of Engineering Mechanics 2002; 128(7):720-729.

[48] Vytiniotis A. Contributions to the analysis and mitigation of liquefaction in loose sand slopes. PhD Thesis. Massachusetts Institute of Technology, 2011.

[49] McGann C, Arduino P, Mackenzie-Helnwein P. InitialStateAnalysisWrapper. http://opensees.berkeley.edu/wiki/index.php/InitialStateAnalysisWrapper; 2011.

[50] Desai C, Nagaraj B. Modeling for cyclic normal and shear behavior of interfaces. Journal of Engineering Mechanics 1988; 114(7):1198-1217.

[51] Elgamal A, Yan L, Yang Z, Conte JP. Three-dimensional seismic response of Humboldt Bay bridge-foundation-ground system. Journal of Structural Engineering 2008; 134(7):1165-1176.

[52] Chiaramonte MM. An analysis of conventional and improved marginal wharves. PhD Thesis, University of Washington, 2011.

[53] Ramanathan K, Jeon JS, Zakeri B, DesRoches R, Padgett JE. Seismic response prediction and modeling considerations for curved and skewed concrete box-girder bridges. Earthquakes and Structures 2015; 9(6):1153-1179.

[54] Medina RA, Krawinkler H. Seismic demands for nondeteriorating frame structures and their dependence on ground motions. PEER Report 2003/15, May, 2004.

[55] Cornell CA, Jalayer F, Hamburger RO, Foutch DA. Probabilistic basis for 2000 SAC federal emergency management agency steel moment frame guidelines. Journal of Structural Engineering 2002; 128(4):526-533.

[56] De Biasio M, Grange S, Dufour F, Allain F, Petre-Lazar I. A simple and efficient intensity measure to account for nonlinear structural behavior. Earthquake Spectra 2014; 30(4):1403-1426.

[57] Urlainis A, Shohet IM, Levy R. Probabilistic risk assessment of oil and gas infrastructures for seismic extreme events. Procedia Engineering 2015; 123:590-598.

[58] International Navigation Association (PIANC). Seismic design guidelines for port structures. A. A. Balkema Publishers, 2001.

Table 1. Physical properties of soil under wharf structure.

Soil unit		Elevation (m)	Soil description	Density, ρ (kg/m^3)	Friction angle, φ (°)	Shear modulus, G (MPa)	Bulk modulus, B (MPa)	Cohesion, c (kPa)
I		52.0~54.2	Sandy fill (above ground water table)	1920				
II	A	45.0~52.0	Loose marine sand	1920	32	100	469	0
II	B	36.0~45.5	Dense marine sand	2000	36	151	703	0
II	C	35.5~39.0	Medium dense marine sand	2000	34	127	591	0
III	A	29.5~37.0	Soft to stiff lagoonal clay	1760	0	26	122	80
III	B1	25.0~29.5	Stiff lagoonal clay	1840	0	43	200	108
III	B2	17.0~25.0	Stiff lagoonal clay	1840	0	84	391	135
IV	A	19.0~22.0	Dense lakewood-San Pedro sand	2000	36	186	868	0
IV	B	0~19.0	Very dense lakewood-San Pedro sand	2080	38	279	1300	0
-	Dike	32.0~52.0	Quarry run	2240	45	141	1363	20

Table 2. Properties of concrete and prestressed steel used in fiber section.

Parameter	Description	Unit	Value
$f_c^{'}$	Concrete compressive strength	MPa	74.9 (49.0)
ε_c	Strain at concrete compressive strength	-	0.005 (0.002)
f_{cu}	Concrete crushing strength	MPa	63.0 (0)
ε_{cu}	Strain at concrete crushing strength	-	0.018 (0.004)
f_y	Steel yield strength,	MPa	1490
E	Steel elastic modulus	MPa	2.04×10^5
σ_{Init}	Prestressing	MPa	1062
B	Steel strain-hardening ratio	-	0

Note: the value outside parentheses represents the properties of confined concrete, while those inside parentheses characterize the properties of unconfined concrete.

Table 3. Bound limits of seismic demand parameters associated with different damage states.

Demand parameters	Slight		Moderate		Extensive	
	With SPI	Without SPI	With SPI	Without SPI	With SPI	Without SPI
Deck displacement, D_{deck} (m)	0.135	0.119	0.250	0.198	0.442	0.283
Bending moment on the Pile F top, $M_{top,\ F}$ (kN-m)	658.5	712.4	748.5	862.0	828.5	993.2
Curvature on the top of Pile F, $\kappa_{top,\ F}$ (1/m)	0.0197	0.0217	0.0386	0.0432	0.0663	0.0761

Note: Bound limits of seismic demand parameters are obtained by pushover analysis.

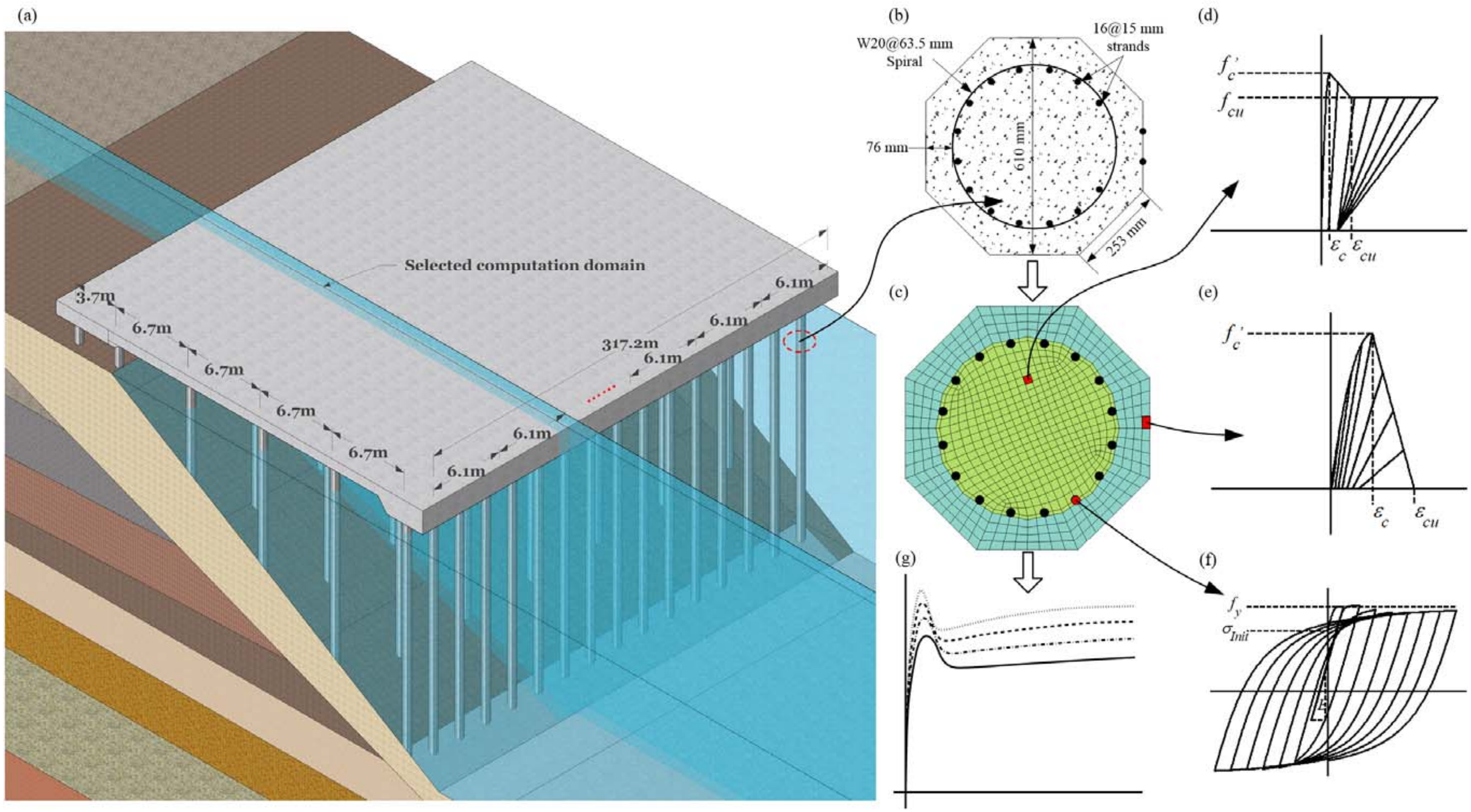

Figure 1. Configuration of wharf structure and pile modeling: (a) 3D view; (b) pile geometry section; (c) fiber discretization of pile cross section; (d) and (e) core and cover Concrete01 Kent-Scott-Park model; (f) Steel02 Giuffre-Menegotto-Pinto model; (g) moment-curvature behavior of prestressed reinforced concrete pile cross section.

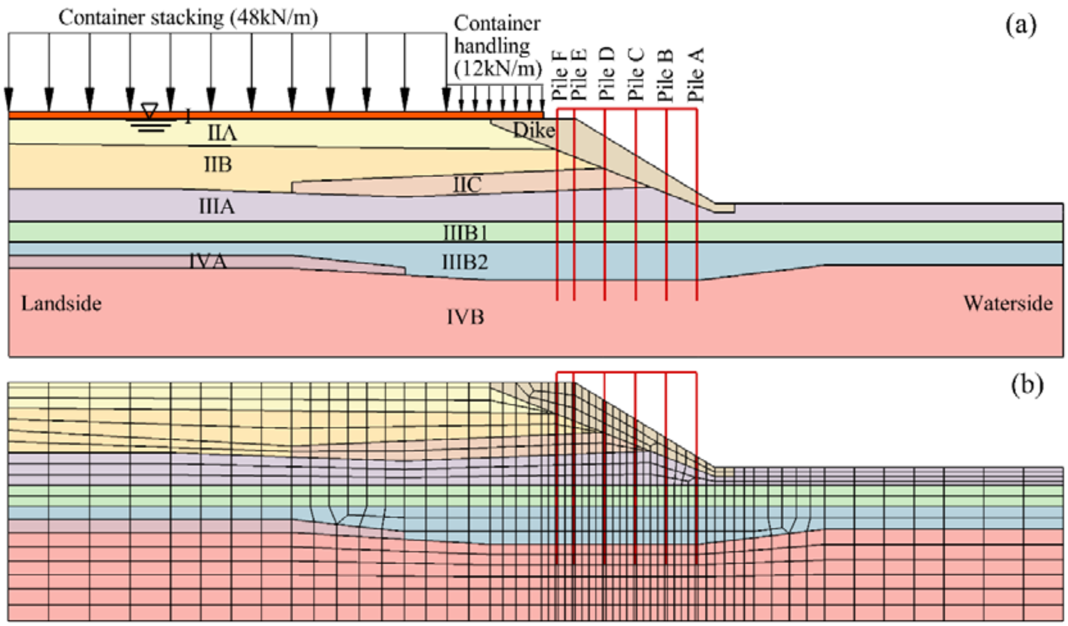

Figure 2. Pile-supported wharf structure: (a) model configuration; (b) finite element mesh.

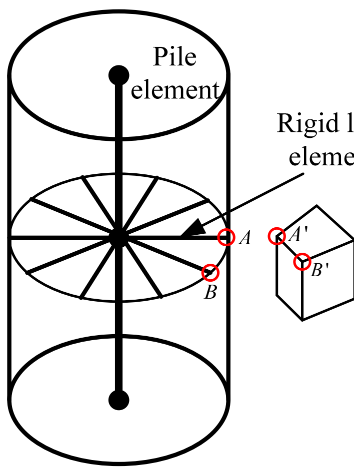

Figure 3. Modeling of soil-pile interaction.

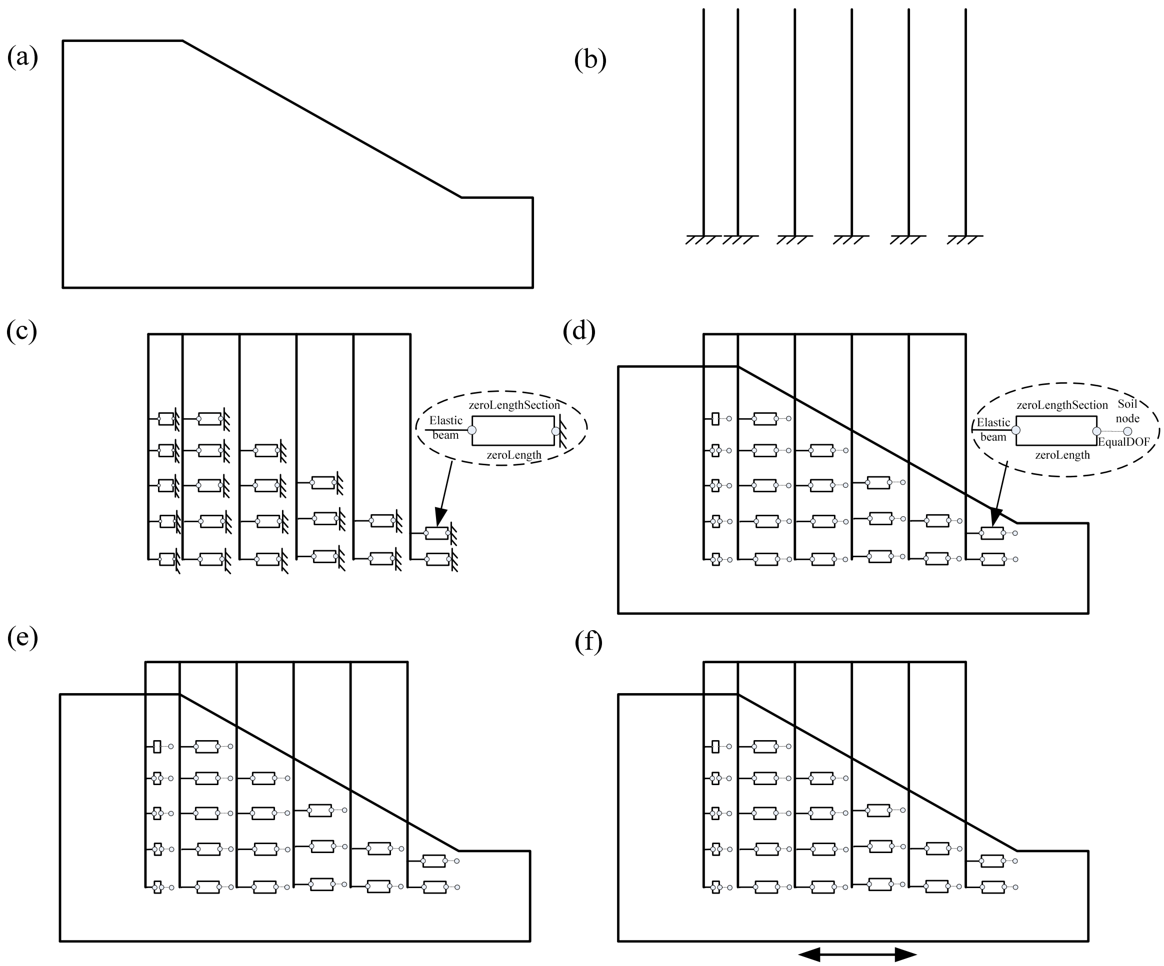

Figure 4. Staged analysis steps of numerical model considering the pile prestressing: (a) soil gravity analysis (Elastic); (b) apply pile prestress; (c) pile connect with elastic and zerolength element; (d) zerolength element connect with soil mesh; (e) switch from elastic to plastic; (f) apply earthquake motion.

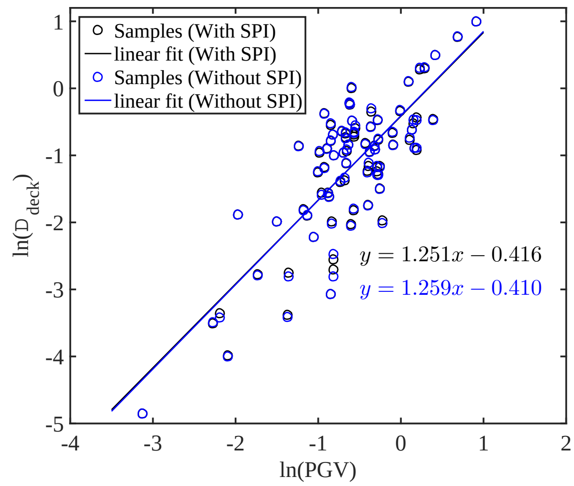

Figure 5. Linear fit demand model of deck displacement.

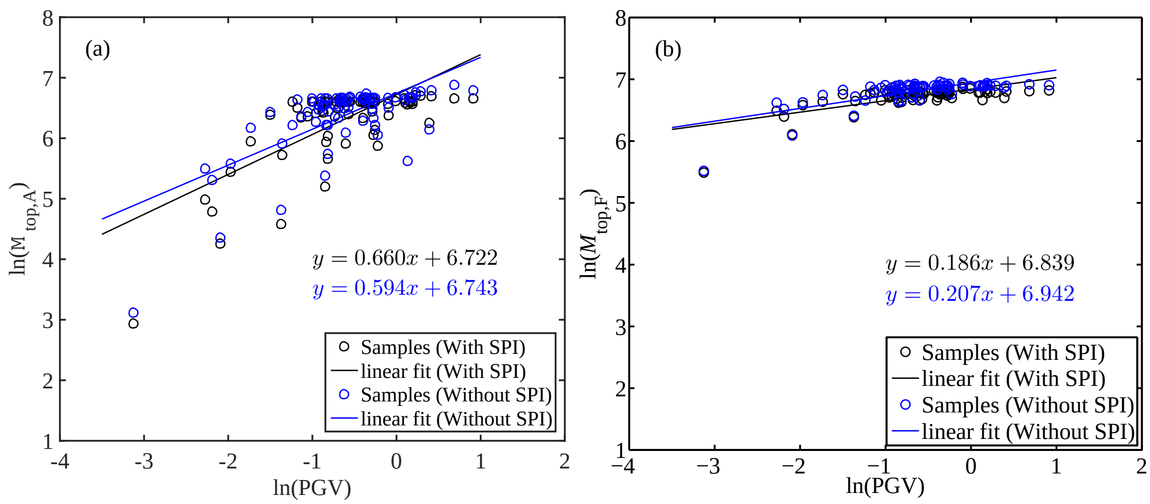

Figure 6. Linear fit demand model of bending moment on pile top: (a) Pile A; (b) Pile F.

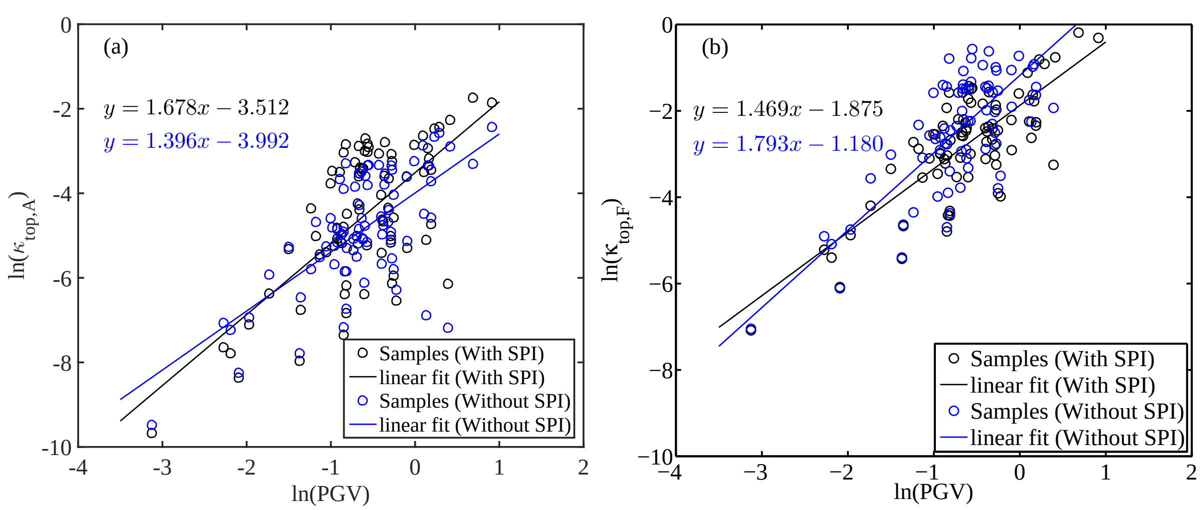

Figure 7. Linear fit demand model of curvature on pile top: (a) Pile A; (b) Pile F.

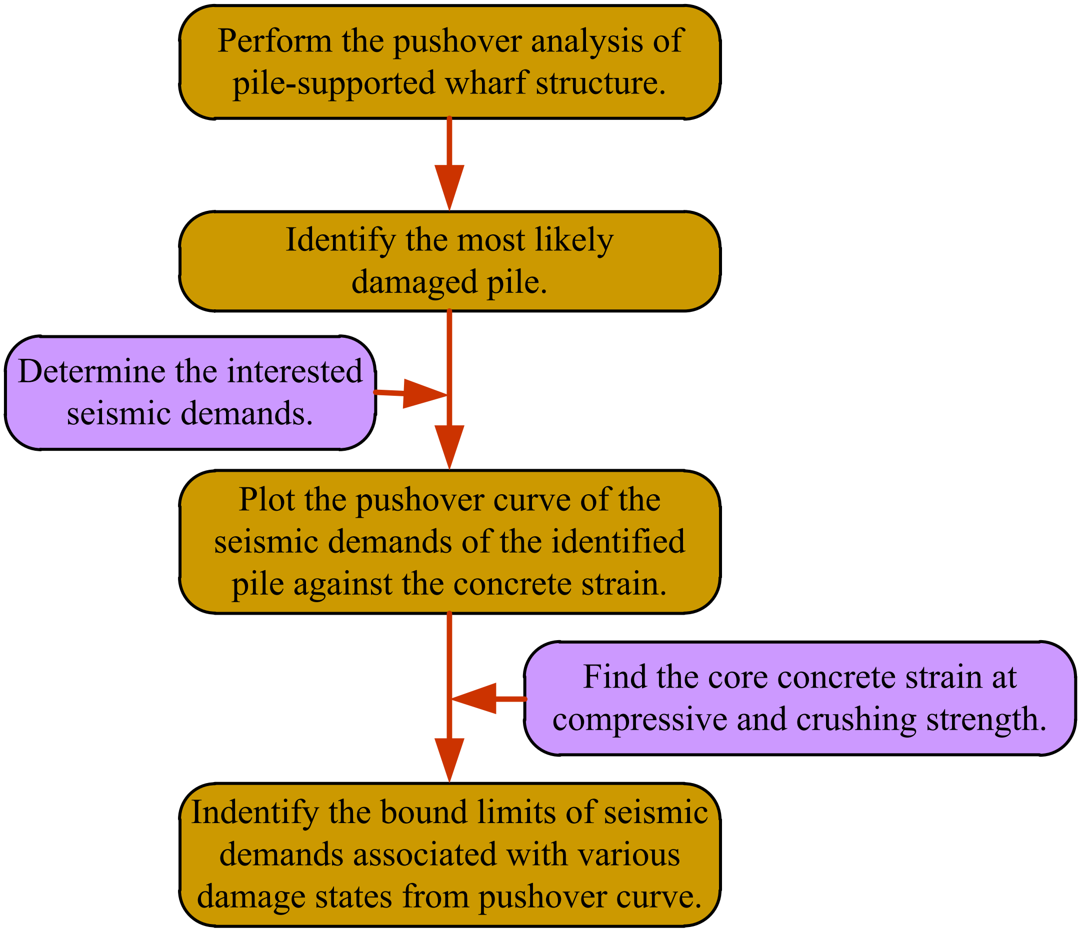

Figure 8. Flowchart of determination of bound limits of seismic demands the PSWS based on pushover analysis.

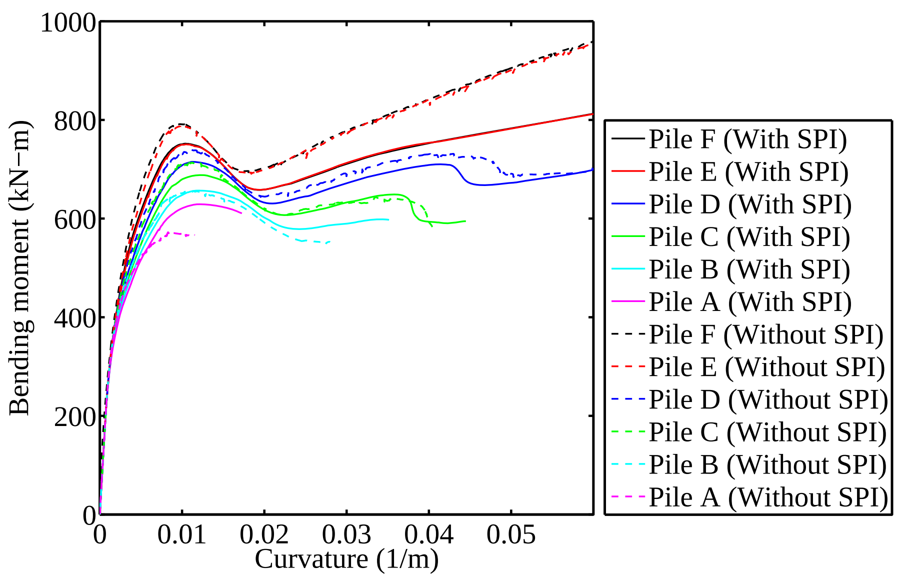

Figure 9. Pushover bending moment-curvature response on pile top.

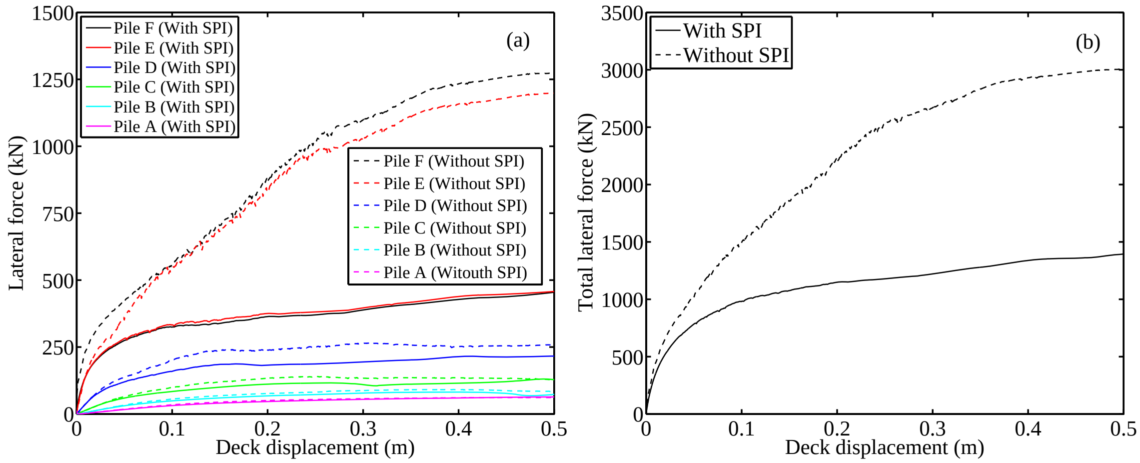

Figure 10. Pushover force-displacement response on pile top: (a) single pile; (b) all piles.

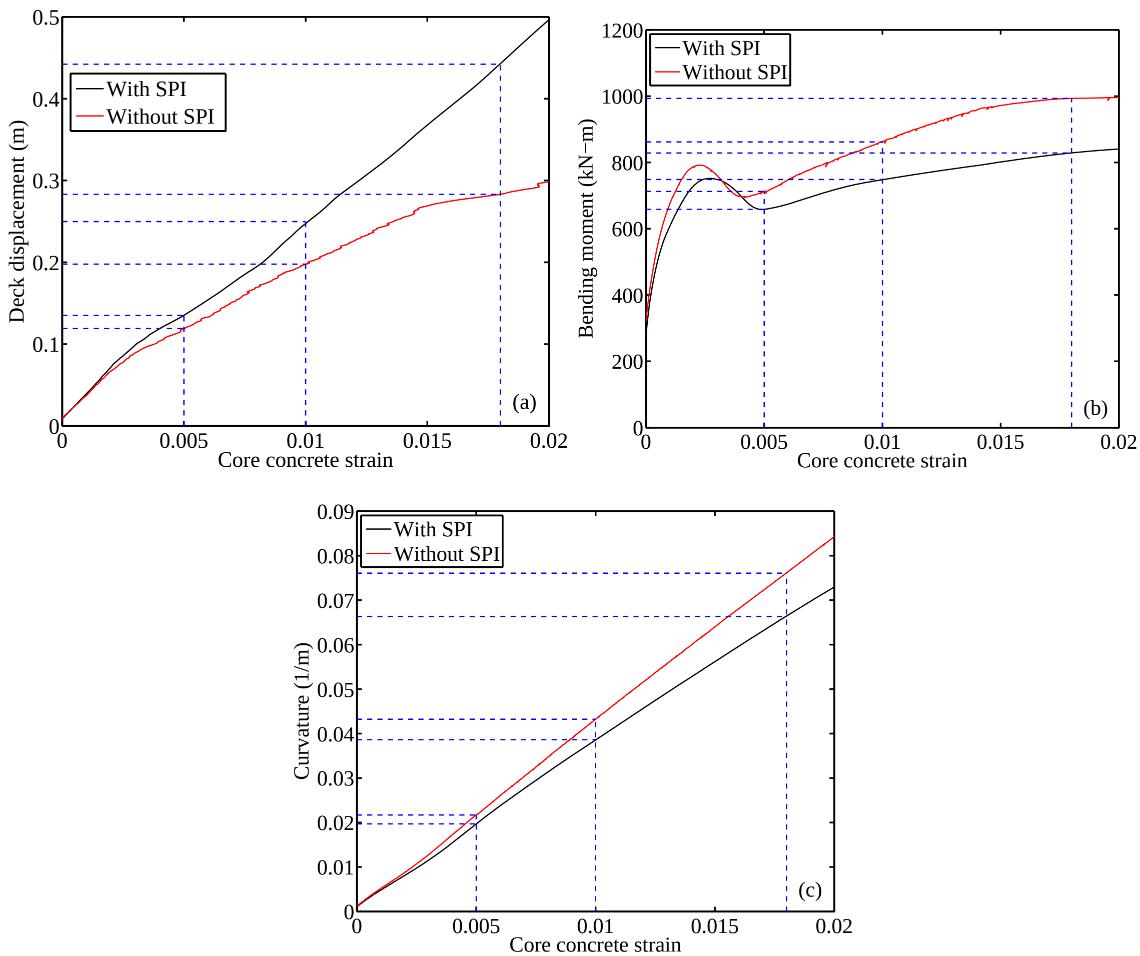

Figure 11. Relationship between the core concrete strain and interested responses on pile F top: (a) deck displacement; (b) bending moment; (c) curvature.

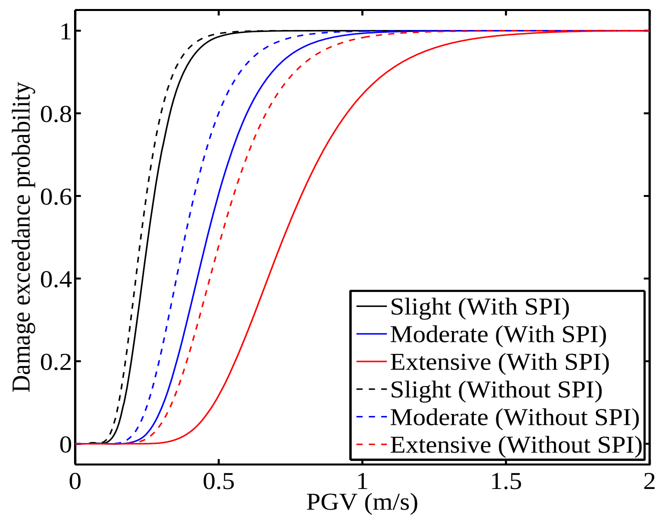

Figure 12. Fragility curves of deck displacement.

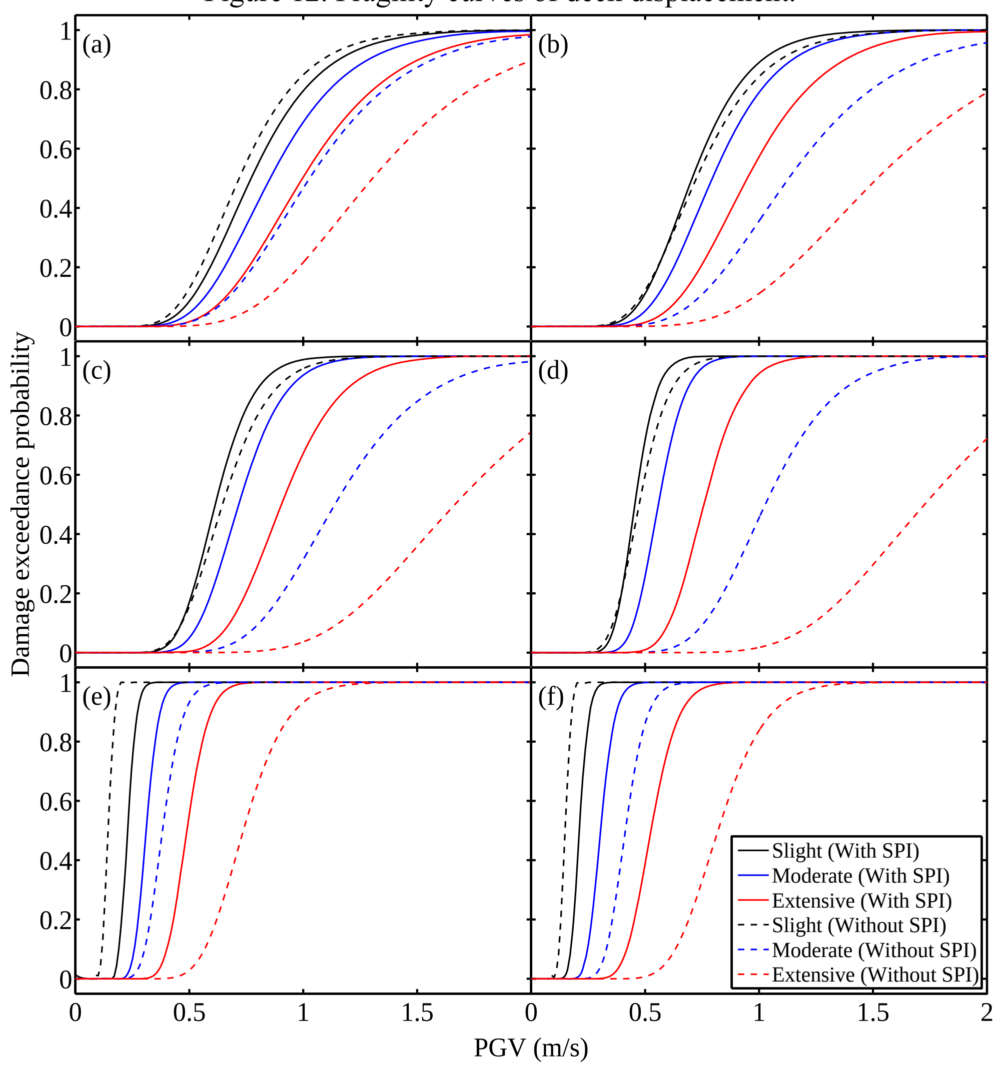

Figure 13. Fragility curves of bending moment on pile top: (a) Pile A; (b) Pile B; (c) Pile C; (d) Pile D; (e) Pile E; (f) Pile F.

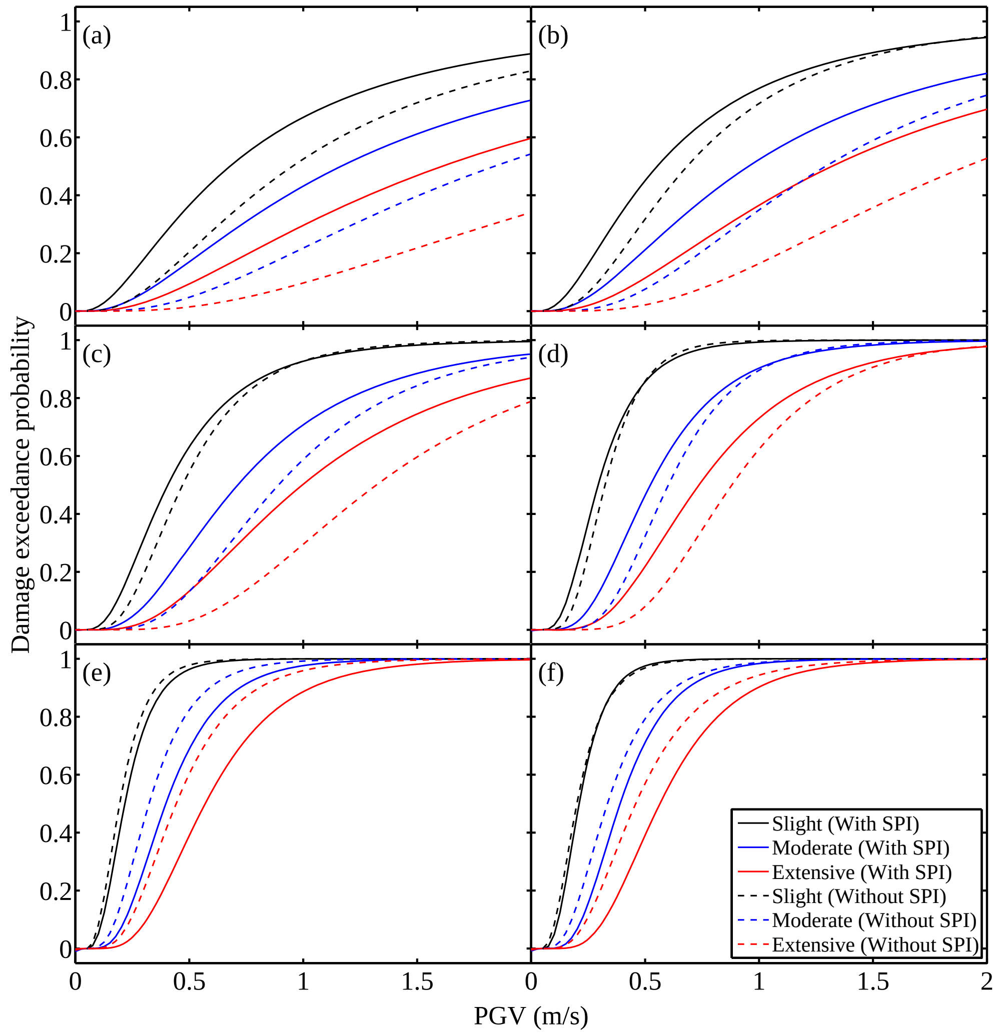

Figure 14. Fragility curves of curvature on pile top: (a) Pile A; (b) Pile B; (c) Pile C; (d) Pile D; (e) Pile E; (f) Pile F.